Influence of end-effect and end-winding on the electromagnetic losses and efficiency in high speed permanent magnet machines

Ahlam Luaibi Shuraiji[1], Sabah A. Gitaffa[2], Kassim Rasheed Hameed[3], Salam Waley Shneen[4]

[1]Electromechanical Engineering Department, University of Technology, Baghdad, Iraq
[2]Electrical Engineering Department, University of Technology, Baghdad, Iraq
[3]Department of Electrical Engineering, College of Engineering, Mustansiriyah University, Baghdad, Iraq
[4]Nanotechnology and advanced material research Center, University of Technology, Baghdad, Iraq

Article Info

ABSTRACT

Permanent-magnet excitation machines (SPMMs) having mounted magnet on the outer surface of their rotor are preferred for high-speed applications such as turbochargers, mechanical turbo-compounding systems, racing engines and fuel pumps, over other types of machines including induction and switched-reluctance machines, since the SPMMs integrate the features of high torque density, compact rotor structure, high reliability and simple structure. However, in the SPMMs, due to the need for a retaining sleeve for the rotor, a large magnetic airgap results and consequently a large magnet thickness is required, hence the magnetic end-effect is relatively high. On the other hand, the use of an overlapping distributed winding leads to a significantly large end-winding length. Hence, the end-effect and the end-winding influences on the performances of a high-speed SPMM is considered in this paper. With a view to get the impact of the end-effect, a comparison between three-dimensional (3D-FEA) results and counterparts two-dimensional finite element analyses (2D-FEA) has been conducted. Results show that, higher efficiency at low torque and low speed due to the low electromagnetic losses and at high speeds due to the high flux-weakening capability are seen when the influences of end-effect as well as end-winding are taken into account.
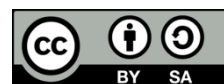
Corresponding Author:

Ahlam Luaibi Shuraiji
Department of Electromechanical Engineering, University of Technology
Baghdad, Iraq
Email: ahlamly2009@yahoo.com, 50053@uotechnology.edu.iq

1. INTRODUCTION

High-speed electrical machines are being applied in considerable industrial applications like turbo-compressors, turbochargers, and engine electrification applications. These machines must be able to accomplish the electromagnetic as well as mechanical requirements at operating conditions of high temperature and high-speed. Therefore, in comparison to the induction and switched-reluctance machines, permanent magnet machines having mounted magnet on the outer surface of their rotor (SPMMs) would be suitable candidates for such applications because they offer the merits of high torque density and a rotor of relative mechanical integrity. Additionally, the SPMMs are distinguished by relatively low electromagnetic losses and high torque capability. Moreover, they are delivering low back-electromotive force (EMF) harmonics and consequently low torque ripple since overlapping distributed winding is normally employed [1]–[4].

However, to insure the rotor mechanical integrity at high speeds operating conditions, a retaining sleeve should be used, this results in a large magnetic airgap. To overcome this, a relatively large permanent magnet thickness is required and consequently a high permanent-magnet-end-leakage is anticipated, i.e. end-effect. Which results in decreasing in the machine electromagnetic performance. Thereby, it has to be considered in performance prediction [5]–[8].

Analytical methods that include the end-effect were reported in [5], [6]. Moreover, a lumped parameter circuit was used to model the leakage flux in the end-region [7]. Despite the fact that in both mentioned methods the results can be predicted relatively quickly, accuracy could be an issue in some applications. Hence, end-effect could be predicted precisely using three-dimensional finite element analysis (3D-FEA), though this method requires significant computing overhead [8]. Furthermore, several research were investigated the impact of the end-effect on the performances of diverse PM machines [9]–[16]. Sanada et al. [9] the impact of the end-effect in high-speed internal PM machine was examined. Polinder et al. [10] introduced an analytical model of a SPMM taking into account the magnetic saturation as well as the end-effect, whereas [11] investigated the influence of the end-effect on the torque-speed profile. In addition, a comparison between 3D and 2D FEA results of doubly-salient machine has been conducted, to highlight the impact of the end-effect [12], [13]. In [14]–[16] lumped-parameter-circuit and 3D-FEA were used to develop and analyse A 3D-model of SFPMM, the model was experimentally validated.

A distributed overlapping winding configuration is preferred over its counterpart concentrated non-overlapping since it results in low back-EMF harmonics and large winding factor [17]. However, such a winding configuration leads to a large coil spin and therefore a large end-winding length and thus a large increase in the copper loss is expected and therefore a significant influence on efficiency. Additionally, the inclusion end-winding in the inductance calculation leads to higher values due to the end-winding and leakage inductances. Therefore, similar to end-effect, neglecting the end-winding influence results in a large error in the predicted results and therefore needs to be considered in performance prediction [18]. Moreover, several studies and investigation focusing on the influence of the end-winding have been conducted [19]–[25]. Ban et al. [19] the end-winding leakage inductance is investigated analytically, and further investigation on the end-winding inductance [20]. Analytical method for leakage inductance considering the end turn shape is proposed in [21], [22]. Calculation methods investigating the effects of the end-winding and end-effect on the machine torque performance in Potgieter and Kamper [23]. Furthermore, the torque-current characteristics are studied with consideration of end-winding is reported in Henneberger et al. [24]. Finally, the influence of the end-winding on the induced eddy current in the end-region of the machine is investigated in Silva et al. [25].

In current paper, the impact of the end-effect as well as the end-winding on the behavior of a high speed SPMM is studied. 2D-FE and 3D-FE models of the under-investigation machine have been achieved by ANSOFT MAXWELL SOFTWARE in order to predict the machine electromagnetic performances including open-circuit results, developed electromagnetic torque, speed-torque curves, the electromagnetic losses and efficiency map. A comparison between the 2D-FEA results and 3D-FEA counterparts is introduced and the reasons for their differences are discussed. Additionally, an individual optimization procedure using 2D- and 3D-FEA is made in order to obtain the influence of the end-effect and end-winding on the optimum design values. Finally, the findings of this paper have been validated experimentally.

2.   SPM MACHINE

SPMM for high-speed application is used in this study. The rotor contains the PM, which is enclosed by a retaining sleeve to preserve the rotor mechanical integrity at high-speeds. However, as stated previously, such a sleeve increases the magnetic airgap which requires an increased magnet thickness and therefore a significant high end-effect can be expected. Conversely, an overlapping distributed winding configuration is employed in order to reduce the back-EMF harmonics and achieve high winding factor. It is worth to mention that the presented results in this paper are per unit values.

3.   INFLUENCE OF END-EFFECT AND END-WINDING ON ELECTROMAGNETIC PERFORMANCE

3.1. Open circuit (O. C.) condition

Figure 1 compares the 2D-FEA normal component of the flux density in the airgap and the 3D-FEA counterpart. For the 3D model, the flux density in the airgap is predicted at the middle of the axial length of the machine as well as at both ends. Clearly, the 2D- and the 3D-FEA results are analogous when the flux density in the airgap is predicted at the middle of the 3D model, Figure 1(a). Whereas, due to the presence of the end leakage, less value and higher airgap flux density distortion can be noted at both ends of the SPPM, Figure 1(b). Likewise, lower back-EMF amplitude and total harmonic distortion (THD) are delivered when

the end-effect is included, Figure 2 in which Figure 2(a) compares the waveforms, while Figure 2(b) compares the FFTs of both 2D and 3D-EFA. This is because of the end permanent magnet leakage, which results in reduction the fundamental and other order harmonics values of the back-EMF at the same average.
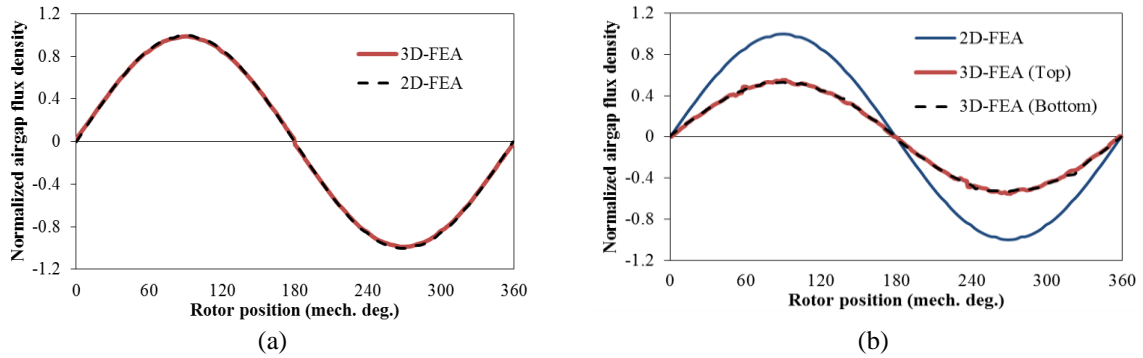

Figure 1. Comparison of 2D-FEA and 3D-FEA flux densities of the airgap at middle of the axial length and both end-regions (a) middle and (b) end-regions
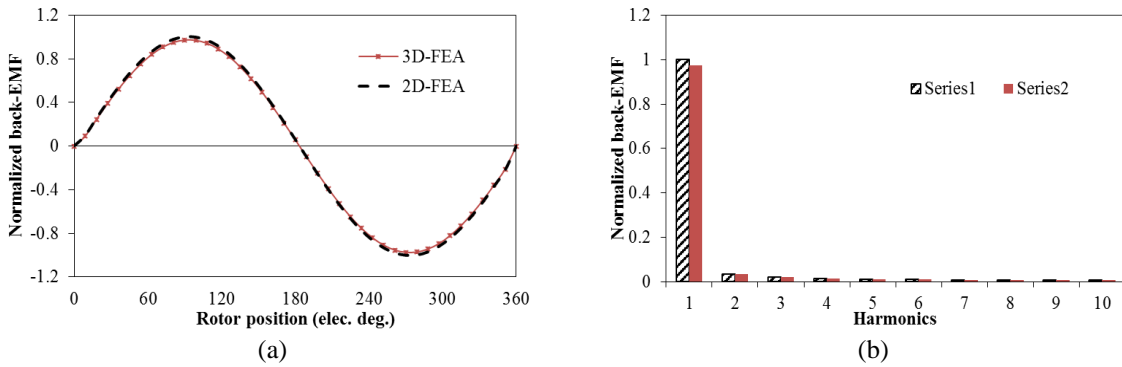

Figure 2. 2D-FEA and 3D-FEA back-EMF waveform and harmonics (a) waveform and (b) harmonics

3.2. Electromagnetic torque

Due to its small saliency ratio, the SPMM possesses a neglected reluctance-torque. Thereby, at constant torque region operating circumstances, the electromagnetic torque of the machine can be found by (1).

$$T_e = \frac{3}{2} N_r \Psi_{pm} I_q \tag{1}$$

Where Nr, Ψ_{PM} and Iq are pole pairs number, flux-linkage of the PM and quadrature-axis current. However, under flux weakening region the torque of SPMM is (2).

$$T_e = \frac{3}{2} N_r (\Psi_{pm} I_q + (L_d - L_q) I_d I_q) \tag{2}$$

Where L_d and L_q are the inductances on the direct- and quadrature-axis, respectively, and I_d stands for direct-axis current. Figure 3 compares the 2D-FEA and 3D-FEA electromagnetic torque of the SPMM under a load condition of (I_q=100A, I_d =0). corresponding to the back-EMF the 2D-FEA torque value is 3% higher than that of the 3D-FEA. Furthermore, the waveform of the torque has considerably low ripples, since the total harmonic distortion of the back-EMF waveform is low, as seen in Figure 2(b). Thereby, the difference in the ripple of the torque between the 2D-FEA and 3D-FEA could be ignored.
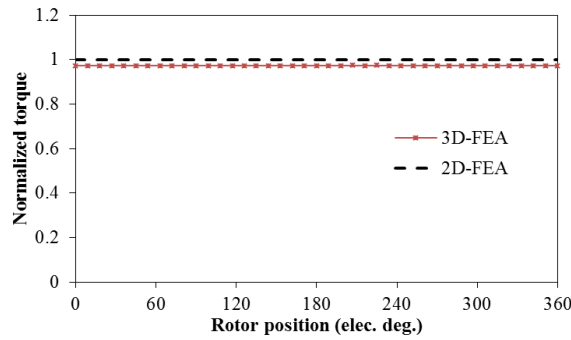
Figure 3. Electromagnetic torque waveforms

4. IMPACT OF END-EFFECT AND END-WINDING ON TORQUE-SPEED CURVE
The (2) and (3) can be used to obtain torque speed characteristics (3).

$$V_{ph} = \sqrt{(R_a I_d - \omega L_q I_q)^2 + (R_a I_q + \omega L_d I_d - \omega \Psi_{pm})^2} \tag{3}$$

Where V_{ph} is the phase-voltage supplied by the inverter and R represents the winding resistance of one phase of the machine. Therefore, in order to analyses the torque-speed curve, PM-flux-linkage and the direct-axis and quadrature-axis inductances are obtained by the 2D-FE and the3D-FE models. The full coupling method proposed in [26] has been applied to consider the magnetic saturation and cross-coupling effects completely.

4.1. Permanent magnet flux Linkage and inductances
Figure 4 introduces the flux linkage of the permanent magnet under different quadrature-axis current levels. The influence of saturation is not significant. Hence, the difference between both 2D-FEA and 3D-FEA is the same at all the current levels. On the other hand, higher values of inductances are delivered by the 3D- compared to their 2D-FEA counterparts as introduced in Table 1. The reason is due to end-winding inductance as well as the leakage inductance.
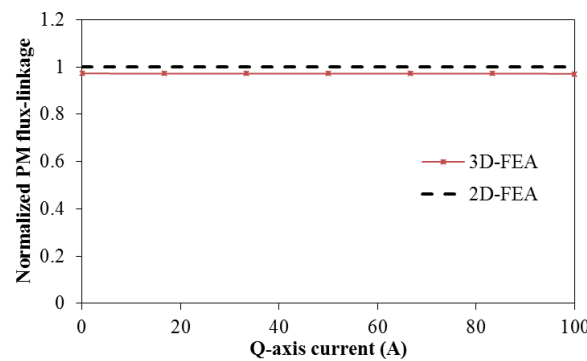

Figure 4. 2D-FEA and 3D-FEA PM-flux-linkage for different quadrature-axis current levels

Table 1. Normalized L_d and L_q for different values of current predict by 2D- and 3D-FEA

Current	D-axis inductance (2D-FEA)	Q-axis inductance (2D-FEA)	D-axis inductance (3D-FEA)	Q-axis inductance (3D-FEA)
$I_q=1, I_d=-100$	1	0.9405	1.219	1.153
$I_q=33, I_d=-83$	1	0.9702	1.219	1.185
$I_q=50, I_d=-50$	1	0.9816	1.217	1.192
$I_q=83, I_d=-33$	1	0.9862	1.215	1.199
$I_q=100, I_d=-1$	0.9977	0.9885	1.203	1.199

4.2. Torque- and power-speed curves

Employing the predicted PM flux-linkage and inductances by FEA in (2) and (3), the torque- and power-speed curves are obtained and shown in Figure 5, where Figure 5(a) is comparing 2D-FEA and 3D-FAE torque-speed profile, while Figure 5(b) presents a compression between 2D-FEA power-speed performance and its 3D counterparts. A lower constant torque region is observed in the 3D-FEA, however a slightly lower base speed and significantly wider flux weakening region is found. The reason is due to higher inductances and lower flux-linkage of the PM, which result in increasing the flux weakening factor [27].
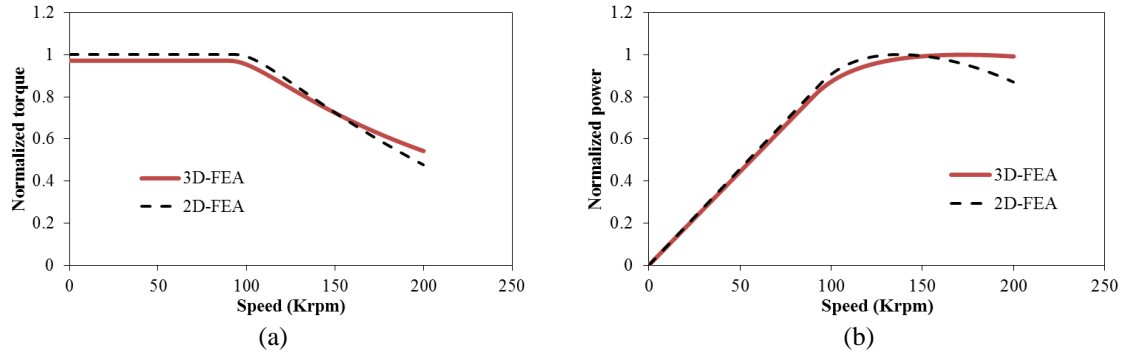

Figure 5. Torque-speed and power-speed curves (a) 2D- and 3D-FEA torque-speed curves and (b) 2D- and 3D-FEA power-speed curves

5. INFLUENCE OF END-EFFECT AND END-WINDING ON ELECTROMAGNETIC LOSSES AND EFFICIENCY

5.1. Copper loss

The DC copper loss in electrical machines is found by (4).

$$P_{DC} = \frac{3I_{ph}^2 N_{ph}^2 \rho_{cu} l_c}{A_s K_p} \qquad (4)$$

Where I_{ph} is the current per phase, N_{ph} represents the turn number per phase, p_{cu} indicates the copper resistivity, l_c referred to the coil length, A_s is the area of the slot, and K_p is for the packing factor. Normally, the length of the coil is calculated analytically since accurate mathematical approaches to obtain the coil spin length are available in literature. The length of the coil including the end-winding spin can be calculated analytically using (5).

$$l_c = 2(l_{ax} + 2\pi \left(\frac{N_{cs}}{N_s}\right)(R_{ins} + l_s) + l_{cb}) \qquad (5)$$

Where l_{ax} is the axial length, N_{cs} is the number of slots of the coil spin, N_s is the number of slots, R_{ins} is the stator inner radius, l_s is the length of the slot, and l_{cb} is the length of the coil bend. When the end-winding length is ignored (2D copper loss), the coil length is equal to twice the axial length of the machine, whereas 3D copper loss is found when the end-winding is considered. However, it is worth to mention that the AC copper loss component which consists of skin and proximity effects is excluded from this study since this machine is modelled with significantly reduced AC loss and therefore it can be neglected.

5.2. Core and rotor losses

Generally, Steinmetz equation, (6) is applied to determine core loss in electrical machines.

$$P_{core} = k_h(B,f) * B * f^2 + k_c(B,f) * B * f \qquad (6)$$

Where B and f are the flux density and frequency, respectively. k_h, and k_c are the hysteresis and eddy factors of the used core material, respectively. Figure 6 presents the core loss of the SPMM at 100 K under different currents. When the current levels are below 100 A, the 3D-FEA predicted core loss is lower than that of the 2D-FEA this is because of the leakage effect, which reduces the magnetic-flux density in the core of the

machine. However, at higher current levels, i.e. above 100 A, due to the influence of the induced flux by the end-winding in the end region of machine the 3D-FEA core loss exceed the 2D-FEA counterpart [25].

On the other hand, the induced eddy current in the conductive components, i.e. magnets, retaining sleeves and shaft, in the SPMM results in induced eddy current loss, such loss can be found by (7).

$$P_{eddy} = \sum_n \left\{ \int_{vol} \frac{|J_n|^2}{2\sigma} dv \right\} \tag{7}$$

Where J and σ represent induced current-density in conductive volume, the material conductivity, respectively. When both end-effect and end-windings are considered, i.e. 3D-FEA, lower eddy losses are observed, as shown in Figure 7. This is because of the both flux-leakages, which includes the end-effect leakage and stator flux-leakage that lead to decrease the induced eddy current and therefore lower loss
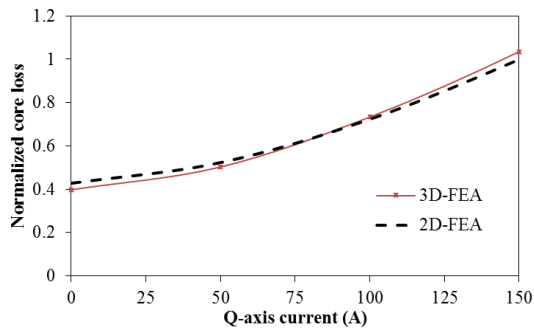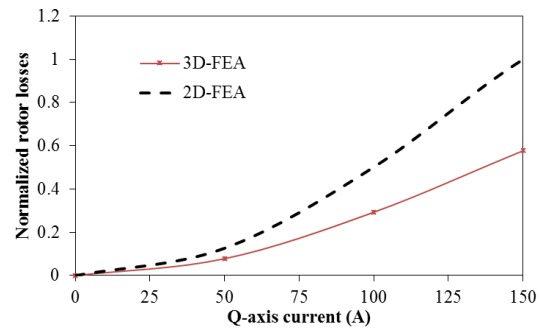

Figure 6. 2D-FEA and 3D-FEA Core loss

Figure 7. 2D-FEA and 3D-FEA rotor losses

5.3. Efficiency map

The efficiency at different current levels and speeds is found by employing the FEA predicted core and rotor losses as well as the calculated copper loss in:

$$\eta = \frac{P_{em} - P_{core} - P_{eddy}}{P_{em} + P_{DC}} \tag{8}$$

where P_{em} is the electromagnetic power ($T_{e\omega}$) Figure 8(a) and Figure 8(b) presents the efficiency map using the core and rotor losses obtained by 2D-FEA and 3D-FEA, respectively. Higher efficiency at lower torques and speeds is observed since lower losses are obtained and since the power level is low therefore the losses influence on the efficiency is noticeable. Additionally, higher efficiency at higher speed levels is found, due to the influence of flux-weakening, since the large inductance increases the output torque and consequently power as well as lower core and magnet losses is observed at these levels due to the influence of flux weakening.
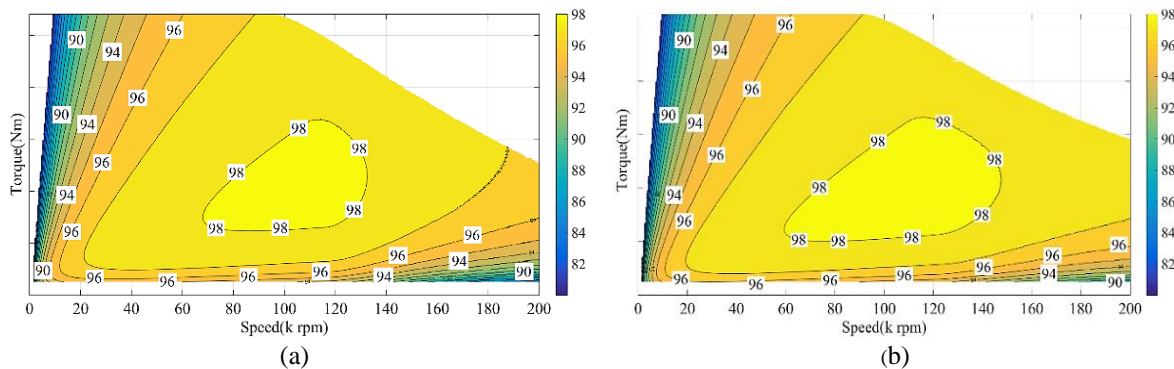

(a)

(b)

Figure 8. Efficiency map for (a) 2D-FEA predicted efficiency and (b) 3D-FEA predicted efficiency

6. CONCLUSION

The impact of the end-effect and end-winding on the open-circuit, developed electromagnetic torque, torque-speed profiles, the electromagnetic losses as well as efficiency on the high-speed SPMM are studied in this paper by the means of 2D-FEA and 3D-FEA. It is found that when such effects are included in the prediction method, lower torque and higher flux weakening capability are observed. On the other hand, higher efficiency at low speeds-low torques and high speeds regions is observed due to the influence of end-effect and end-winding on the core and magnet losses, and the flux weakening capability.

REFERENCES

[1] J. Wang, Z. Ping Xia and D. Howe, "Three-phase modular permanent magnet brushless machine for torque boosting on a down-seized ICE vehicles," *IEEE Trans. Veh. Technol.*, vol. 54, no. 3, pp. 809–816, May 2005, doi: 10.1109/TVT.2005.847224.

[2] A. M. El-Refaie and T. M. Jahns, "Optimal flux weakening in surface PM machines using concentrated windings," *Conference Record of the 2004 IEEE Industry Applications Conference, 2004. 39th IAS Annual Meeting.*, 2004, pp. 1038–1047, vol. 2, doi: 10.1109/IAS.2004.1348541.

[3] A. Vagati, G. Pellegrino and P. Guglielmi, "Comparison between SPM and IPM motor drives for EV application," *The XIX International Conference on Electrical Machines - ICEM 2010*, 2010, pp. 1–6, doi: 10.1109/ICELMACH.2010.5607911.

[4] J. Wang, X. Yuan and K. Atallah, "Design optimization of a surface-mounted permanent-magnet motor with concentrated windings for electric vehicle applications," in *IEEE Transactions on Vehicular Technology*, vol. 62, no. 3, pp. 1053–1064, March 2013, doi: 10.1109/TVT.2012.2227867.

[5] J. Azzouzi, G. Barakat and B. Dakyo, "Quasi-3-D analytical modeling of the magnetic field of an axial flux permanent-magnet synchronous machine," in *IEEE Transactions on Energy Conversion*, vol. 20, no. 4, pp. 746–752, Dec. 2005, doi: 10.1109/TEC.2005.845538.

[6] Y. Chen, Z. Q. Zhu and D. Howe, "Three-dimensional lumped-parameter magnetic circuit analysis of single-phase flux-switching permanent-magnet motor," in *IEEE Transactions on Industry Applications*, vol. 44, no. 6, pp. 1701–1710, Nov.-dec. 2008, doi: 10.1109/TIA.2008.2006352.

[7] M. Platen and G. Henneberger, "Examination of leakage and end effects in a linear synchronous motor for vertical transportation by means of finite element computation," *in IEEE Transactions on Magnetics*, vol. 37, no. 5, pp. 3640–3643, Sept. 2001, doi: 10.1109/20.952680.

[8] C. Zhao, S. Li and Y. Yan, "Influence factor analysis of PMSM air gap flux density," *2005 International Conference on Electrical Machines and Systems*, 2005, pp. 334–339, vol. 1, doi: 10.1109/ICEMS.2005.202541.

[9] M. Sanada, S. Morimoto and Y. Takeda, "Interior permanent magnet linear synchronous motor for high-performance drives," in *IEEE Transactions on Industry Applications*, vol. 33, no. 4, pp. 966–972, July-Aug. 1997, doi: 10.1109/28.605738.

[10] H. Polinder, J. G. Slootweg, M. J. Hoeijmakers and J. C. Compter, "Modelling of a linear PM machine including magnetic saturation and end effects: Maximum force to current ratio," *IEEE International Electric Machines and Drives Conference, 2003. IEMDC'03.*, 2003, pp. 805–811, vol. 2, doi: 10.1109/IEMDC.2003.1210328.

[11] W. Hua, M. Cheng, X. Zhu and J. Zhang, "Investigation of end-effect in brushless machines having magnets in the stator with doubly salient structure," *2006 IEEE International Magnetics Conference (INTERMAG)*, 2006, pp. 197–197, doi: 10.1109/INTMAG.2006.375780.

[12] X. Zhu, M. Cheng, W. Hua and J. Zhang, "Investigation of end-effect and experimental validation for hybrid excited doubly salient machine," *2006 12th Biennial IEEE Conference on Electromagnetic Field Computation*, 2006, pp. 320–320, doi: 10.1109/CEFC-06.2006.1633110.

[13] Z. Q. Zhu, J. T. Chen, Y. Pang, D. Howe, S. Iwasaki and R. Deodhar, "Modeling of end-effect in flux-switching permanent magnet machines," *2007 International Conference on Electrical Machines and Systems (ICEMS)*, 2007, pp. 943–948, doi: 10.1109/ICEMS12746.2007.4412225.

[14] Z. Q. Zhu, Y. Pang, W. Hua, M. Cheng, and D. Howe, "Investigation of end effect in permanent magnet brushless machines having magnets on the stator," *Journal of Applied Physics*, vol. 99, no.8, R319, 2006, doi: 10.1063/1.2172182.

[15] Z. Q. Zhu and Z. Azar, "Influence of end-effect and cross-coupling on torque-speed characteristics of switched flux permanent magnet machines," *8th International Conference on Power Electronics - ECCE Asia*, 2011, pp. 145–152, doi: 10.1109/ICPE.2011.5944568.

[16] S. Morimoto, M. Sanada and Y. Takeda, "Effects and compensation of magnetic saturation in flux-weakening controlled permanent magnet synchronous motor drives," in *IEEE Transactions on Industry Applications*, vol. 30, no. 6, pp. 1632-, Nov. 1994, doi: 10.1109/TIA.1994.350318.

[17] A. M. El-Refaie and T. M. Jahns, "Comparison of synchronous PM machine types for wide constant-power speed range operation," *Fourtieth IAS Annual Meeting. Conference Record of the 2005 Industry Applications Conference, 2005.*, 2005, pp. 1015–1022, vol. 2, doi: 10.1109/IAS.2005.1518478.

[18] Y. Zhao, B. Yan, C. Chen, J. Deng and Q. Zhou, "Parametric study on dynamic characteristics of turbogenerator stator end winding," in *IEEE Transactions on Energy Conversion*, vol. 29, no. 1, pp. 129–137, March 2014, doi: 10.1109/TEC.2013.2294334.

[19] D. Ban, D. Zarko and I. Mandic, "Turbogenerator end-winding leakage inductance calculation using a 3-D analytical approach based on the solution of Neumann Integrals," in *IEEE Transactions on Energy Conversion*, vol. 20, no. 1, pp. 98–105, March 2005, doi: 10.1109/TEC.2004.837300.

[20] M. F. Hsieh, Y. -C. Hsu, D. G. Dorrell and K. -H. Hu, "Investigation on end winding inductance in motor stator windings," in *IEEE Transactions on Magnetics*, vol. 43, no. 6, pp. 2513–2515, June 2007, doi: 10.1109/TMAG.2007.896209.

[21] T. Cox, F. Eastham and J. Proverbs, "End turn leakage reactance of concentrated modular winding stators," in *IEEE Transactions on Magnetics*, vol. 44, no. 11, pp. 4057–4061, Nov. 2008, doi: 10.1109/TMAG.2008.2002382.

[22] R. Lin and A. Arkkio, "Calculation and analysis of stator end-winding leakage inductance of an induction machine," in *IEEE Transactions on Magnetics*, vol. 45, no. 4, pp. 2009–2014, April 2009, doi: 10.1109/TMAG.2008.2010317.

[23] J. H. J. Potgieter and M. J. Kamper, "Calculation methods and effects of end-winding inductance and permanent-magnet end flux on performance prediction of nonoverlap winding permanent-magnet machines," in *IEEE Transactions on Industry Applications*, vol. 50, no. 4, pp. 2458–2466, July-Aug. 2014, doi: 10.1109/TIA.2013.2295468.

[24] G. Henneberger, S. Domack and J. Berndt, "Influence of end winding leakage in permanent magnet excited synchronous machines with asymmetrical rotor design," *1993 Sixth International Conference on Electrical Machines and Drives (Conf. Publ. No. 376)*, 1993, pp. 305–311.

[25] V. C. Silva, G. Meunier and A. Foggia, "A 3D finite-element computation of eddy currents and losses in the stator end laminations of large synchronous machines," in *IEEE Transactions on Magnetics*, vol. 32, no. 3, pp. 1569–1572, May 1996, doi: 10.1109/20.497551.

[26] G. Qi, J. T. Chen, Z. Q. Zhu, D. Howe, L. B. Zhou and C. L. Gu, "Influence of skew and cross-coupling on flux-weakening performance of permanent-magnet brushless AC machines," in *IEEE Transactions on Magnetics*, vol. 45, no. 5, pp. 2110–2117, May 2009, doi: 10.1109/TMAG.2009.2013244.

[27] W. L. Soong, and T. J. E. Miller, "Field-weakening performance of brushless synchronous AC motor drive," *IEE Proc. Elect. Power Appl.,* vol. 141, no. 6, pp. 331–340, November 1994, doi: 10.1049/ip-epa:19941470.

BIOGRAPHIES OF AUTHORS

Ahlam Luaibi Shuraiji [ID] [img] [SC] [img] received the B.Eng. and M.Sc. degrees in Engineering Educational Technology/Electrical Engineering, from University of Technology, Baghdad, Iraq, in 1998 and 2004, respectively, and the Ph.D. degree in electrical engineering from The University of Sheffield, Sheffield, U.K., in 2017. She is currently a lecturer at the University of Technology/ Electromechanical Engineering department. Her research interests include the design of permanent-magnet machines. She can be contacted at email: ahlamly2009@yahoo.com.

Sabah A. Gitaffa [ID] [img] [SC] [img] learned his MS.C. in the field of Electronic Engineering from University of Technology. Baghdad-Iraq, 2004. He has more than ten years of experience in teaching. His research interests include, control sensor system, robotic engineering and smart system, MOSFET miniaturization design. He can be contacted at email: 30094@uotechnology.edu.iq.

Kassim Rasheed Hameed [ID] [img] [SC] [img] was born in 1960. He has received B.Sc. in Electrical Engineering in 1983, M.Sc. in electrical Engineering/Transformer Specialization in 2000 from the University of Technology/Baghdad and Ph.D. in Electrical Engineering/Transformer Specialization in 2007 from the University of Technology/Baghdad. From 1987-2007 he worked in the field of manufacturing, Testing and designing electrical transformers at Diyala Company for Transformer Industries in Iraq. He is currently working as an assistant professor in the Department of Electrical Engineering/College of Engineering/Al-Mustansiriya University since 2008. His research interest's High Frequency, Low Frequency Transformer Design and electromagnetic analysis. He has published 8 journal articles. He can be contacted at email: kassim.r.h60@uomustansiriyah.edu.iq.

Salam Waley Shneen [ID] [img] [SC] [img], Educational Background: Jul 2016 PhD, Degree in Electrical Engineering-Power Electronic, School of Electrical and Electronic Engineering, Huazhong University of Science and Technology (HUST). Nov 2005 MSc, Degree in Engineering Educational Technology-Electrical Engineering, Technical Education Department, University of Technology, Iraq-Baghdad. July 1998 BSc, Degree in Electrical Engineering and Education, Technical Education Department, University of Technology, Iraq-Baghdad. Oct 1994 Diploma in Electrical Technology. Assistant Lecturer in: Electronic Lab., Lecturer Advanced Electronic, Lecturer Fundamental of Electric Engineering, Technical Education Department, Electromechanical Department University of Technology, Iraq-Baghdad. 2016-2017 Lecturer in: Electronic Lab. Fundamental of Electric Engineering Lab., Lecturer Electronic Circuits, Lecturer Fundamental of Electric Engineering with Electrical and Electronic Circuits Electromechanical Department University of Technology, Iraq-Baghdad. 2017-10Apr. 2022 Lecturer in: Energy and Renewable Energies Technology Center, University of Technology, Iraq-Baghdad. 10Apr. 2022- today Lecturer in: Nanotechnology and advanced material research Center, University of Technology, Iraq-Baghdad. He can be contacted at email: Salam.w.shneen@uotechnology.edu.iq.